NAVAL POSTGRADUATE SCHOOL

MONTEREY, CALIFORNIA

THESIS

LARGE-SCALE COHERENT FLOW STRUCTURES IN A NATURAL BRAIDED REACH SECTION OF A GRAVEL-BED RIVER

by

William F. Ashley

June 2011

Thesis Advisor:	Jamie MacMahan
Second Reader:	Edward Thornton

Approved for public release; distribution is unlimited

THIS PAGE INTENTIONALLY LEFT BLANK

REPORT DOCUMENTATION PAGE			*Form Approved OMB No. 0704-0188*
Public reporting burden for this collection of information is estimated to average 1 hour per response, including the time for reviewing instruction, searching existing data sources, gathering and maintaining the data needed, and completing and reviewing the collection of information. Send comments regarding this burden estimate or any other aspect of this collection of information, including suggestions for reducing this burden, to Washington headquarters Services, Directorate for Information Operations and Reports, 1215 Jefferson Davis Highway, Suite 1204, Arlington, VA 22202-4302, and to the Office of Management and Budget, Paperwork Reduction Project (0704-0188) Washington DC 20503.			
1. AGENCY USE ONLY ***(Leave blank)***	**2. REPORT DATE** June 2011	**3. REPORT TYPE AND DATES COVERED** Master's Thesis	
4. TITLE AND SUBTITLE Large-Scale Coherent Flow Structures in a Natural Braided Reach Section of a Gravel-Bed River			**5. FUNDING NUMBERS**
6. AUTHOR(S) William F Ashley			
7. PERFORMING ORGANIZATION NAME(S) AND ADDRESS(ES) Naval Postgraduate School Monterey, CA 93943-5000			**8. PERFORMING ORGANIZATION REPORT NUMBER**
9. SPONSORING /MONITORING AGENCY NAME(S) AND ADDRESS(ES) N/A			**10. SPONSORING/MONITORING AGENCY REPORT NUMBER**
11. SUPPLEMENTARY NOTES The views expressed in this thesis are those of the author and do not reflect the official policy or position of the Department of Defense or the U.S. Government.			
12a. DISTRIBUTION / AVAILABILITY STATEMENT Approved for public release; distribution is unlimited			**12b. DISTRIBUTION CODE**

13. ABSTRACT (maximum 200 words)

Stream-wise length scales of coherent flow structures were examined to test the hypothesized 2 to 6 times the depth scale in relatively deeper (~1 *m*) and faster (~1.5 *m/s*) flows in a braided reach of the Kootenai River, Idaho. Velocities were measured using a custom Acoustic Doppler Current Profiler, an array of six electromagnetic current meters, and an Acoustic Doppler Velocimeter in a variety of river depths (0.6–1.7 *m*) and velocities (0.3–1.6 *m/s*). Energetic (50% of total energy), coherent (along the array), low-frequency (< 0.05 *Hz*) motions were found for all deployment locations. Coherent times and lengths were 5 *s* and 10 *m* in the ~1.5 *m/s* flows and 45 *s* and 22 *m* in the ~0.5 *m/s* flows. Multi-resolution decomposition provided coarse low-frequency limit for the coherent motions and suggests the temporal scales range from 10 to 1000 *s*. Length scales of the low-frequency motions determined by frequency-wavenumber spectra indicate that the motions are longer than hypothesized. The coherent times and lengths were consistently less than the computed time and length scales, suggesting the energetic low-frequency motions evolve as they propagate downstream.

14. SUBJECT TERMS Coherent Flow Structures, Gravel-Bed River, River Turbulence, Frequency-Wavenumber Analysis, Multi-Resolution Decomposition			**15. NUMBER OF PAGES** 67
			16. PRICE CODE
17. SECURITY CLASSIFICATION OF REPORT Unclassified	**18. SECURITY CLASSIFICATION OF THIS PAGE** Unclassified	**19. SECURITY CLASSIFICATION OF ABSTRACT** Unclassified	**20. LIMITATION OF ABSTRACT** UU

NSN 7540-01-280-5500

Standard Form 298 (Rev. 2-89)
Prescribed by ANSI Std. 239-18

THIS PAGE INTENTIONALLY LEFT BLANK

Approved for public release; distribution is unlimited

LARGE-SCALE COHERENT FLOW STRUCTURES IN A NATURAL BRAIDED REACH SECTION OF A GRAVEL-BED RIVER

William F. Ashley
Lieutenant, United Stated Navy
B.S., Old Dominion University, 2005

Submitted in partial fulfillment of the
requirements for the degree of

MASTER OF SCIENCE IN PHYSICAL OCEANOGRAPHY

from the

NAVAL POSTGRADUATE SCHOOL
June 2011

Author: William F. Ashley

Approved by: Jamie MacMahan
Thesis Advisor

Edward Thornton
Second Reader

Jeffrey D. Paduan
Chairman, Department of Oceanography

THIS PAGE INTENTIONALLY LEFT BLANK

ABSTRACT

Stream-wise length scales of coherent flow structures were examined to test the hypothesized 2 to 6 times the depth scale in relatively deeper (~1 *m*) and faster (~1.5 *m/s*) flows in a braided reach of the Kootenai River, Idaho. Velocities were measured using a custom Acoustic Doppler Current Profiler, an array of six electromagnetic current meters, and an Acoustic Doppler Velocimeter in a variety of river depths (0.6–1.7 *m*) and velocities (0.3–1.6 *m/s*). Energetic (50% of total energy), coherent (along the array), low-frequency (< 0.05 *Hz*) motions were found for all deployment locations. Coherent times and lengths were 5 *s* and 10 *m* in the ~1.5 *m/s* flows and 45 *s* and 22 *m* in the ~0.5 *m/s* flows. Multi-resolution decomposition provided coarse low-frequency limit for the coherent motions and suggests the temporal scales range from 10 to 1000 *s*. Length scales of the low-frequency motions determined by frequency-wavenumber spectra indicate that the motions are longer than hypothesized. The coherent times and lengths were consistently less than the computed time and length scales, suggesting the energetic low-frequency motions evolve as they propagate downstream.

THIS PAGE INTENTIONALLY LEFT BLANK

TABLE OF CONTENTS

THIS PAGE INTENTIONALLY LEFT BLANK

LIST OF FIGURES

LIST OF TABLES

THIS PAGE INTENTIONALLY LEFT BLANK

LIST OF ACRONYMS AND ABBREVIATIONS

ADCP	Acoustic Doppler Current Profiler
ADV	Acoustic Doppler Velocimeter
DOF	Degrees of Freedom
ECM	Electromagnetic Current Meter
f-k_s	Frequency-Wavenumber
GPS	Global Positioning System
IMLE	Iterative Maximum Likelihood Estimator
MR	Multi-Resolution Decomposition
ONR	Office of Naval Research

THIS PAGE INTENTIONALLY LEFT BLANK

ACKNOWLEDGMENTS

I would like to express my sincere appreciation and gratitude to Professor Jamie MacMahan for his guidance and patience. I feel fortunate to have been your student. I thank Professor Ed Thornton for his insight and additional guidance. I also thank Professor Ad Reniers for his help, time, and hospitality. I thank the Kootenai Tribe of Idaho for their support and continued work to protect their river. A special thanks to the Kootenai field group: Bill Swick, Jenna Brown, Patrick Rynne, and Chris Tuggle. Lastly, but most importantly, I thank my wife, Kelley, and my children for their support, dedication, and understanding.

This study was supported by the Office of Naval Research Coastal Geosciences Program.

THIS PAGE INTENTIONALLY LEFT BLANK

I. INTRODUCTION

Flow in a gravel-bed river appears to be random and chaotic, but through laboratory and field experiments, it has been shown that it is possible to classify the flow into organized motions (Cantwell 1981; Roy et al. 2004), which possess spatial and temporal coherence (Adrian 2007). An understanding of river flow characteristics is important for describing river morphology, bed-load transport (Robert et al. 1996), and mixing. River flow is generally divided into three vertical layers: 1) the near-wall bottom boundary consisting of less than 10% of the flow depth; 2) the outer flow region containing the largest percentage of flow; and 3) the near-surface region (Tamburrino and Gulliver 1999). The two main mechanisms believed responsible for generating large-scale coherent flow structures are turbulence, as a result of bed topography in the near-wall region interacting with the outer flow region (Hardy et al. 2010), and coalescence of vortices generated from prominent river structures (Cantwell 1981). Near-bed turbulence can produce coherent flow structures during a bursting (upwelling) event, where low speed fluid is ejected into the outer flow region that persist until a sweeping (downwelling) event returns high speed flow energy to the near-wall boundary layer (Hardy et al. 2009). In the wake of river features, such as large pebble clusters, riffle pools, or protruding structures, vertical and horizontal eddies are produced at a constant rate and combine to produce large-scale coherent flow structures (Buffin-Belanger and Roy 1998; Cantwell 1981). In both cases, the structures have been described as recurrent patterns of alternating high and low speed wedges (Buffin-Belanger et al. 2000), repetitive quasi-cyclic large-scale turbulent motions, or simply, rolling vortices that move downstream at flow velocity (Shvidchenko and Pender 2001).

Coherent flow structure size is believed to be controlled by flow depth, and experiments using flow visualization techniques and field measurement analysis usually provide size scales as a function of flow depth (e.g., Shvidchenko and Pender 2001; Roy et al. 2004). Since temporal coherence is a prerequisite for identifying a coherent

flow structure (Adrian 2007), the length scale is commonly estimated using Taylor's frozen turbulence hypothesis in which

$$L = UT \,, \tag{1}$$

where U is the mean flow velocity and T is the time-scale, or average period, of the motion (Soulsby, 1980). Zaman and Hussain (1981) concluded Taylor's hypothesis is acceptable for application to large-scale coherent flow structures. Most studies consistently find that the vertical scale of coherent flow structures is proportional to flow depth, but the horizontal length scales, at least in the stream-wise direction, have not been precisely defined. Most studies provide a mean lateral, or cross-stream, width scale of 1 to 2*h*, where *h* is the flow depth, and a mean longitudinal, or stream-wise, length scale of 2 to 6*h* (Marquis and Roy 2006). Shvidchenko and Pender (2001) using flow visualization, quadrant analysis, and energy estimates reported a mean stream-wise length scale of 4 to 5*h* for coherent flow structures in a laboratory flume study. Roy et al. (2004), amongst others, used several techniques described by Nakagawa and Nezu (1981) on field measurements acquired in rivers with similar velocities (<0.5 *m/s*) and depths (<0.5 *m*) and found a 3 to 5*h* length scale. Dinehart (1999) conducted one of the few known coherent flow structure studies in a gravel-bed river with a relatively fast (2 *m/s*) and deep flow (1.5 *m*) using 14.3 *m* instrument separation. He found coherent times of 10 to 30 *s* with lengths of coherent flow structures, termed correlated stream-wise eddies, ranging from 20 to 30 *m* that correspond to a 13 to 20*h* scale. These longer length scales for coherent flow structures in a deeper and faster flow and the range of postulated length scales from others, points out the need for a detailed study in which measurements are collected in a range of depths and flow velocities.

Two common techniques to identify coherent flow structures are deploying either synchronous lagged instrument arrays (e.g., Roy et al. 2004) or separated individual instruments placed some distance apart (e.g., Dinehart 1999). Both techniques measure stream-wise velocities and various methods are applied to estimate the coherence between sensors associated with the passage of a flow structure. A synchronous lagged instrument array is required to describe coherent flow structures, but this requires cabling and limits the array length. It is also limited by the number of

expensive sensors in the array, sensor placement, and the requirement of a frame assembly to mount the sensors, cables, data logger, and power source in the river at fixed locations while minimizing flow disturbance. These limitations have constrained previous studies to laboratory or shallow water field experiments that allow for shorter arrays.

The objective of this study is to measure stream-wise length scales of large-scale coherent flow structures in deeper and faster flow conditions of a gravel-bed river. This study was conducted as part of a research initiative sponsored by the Office of Naval Research (ONR) to investigate the sensitivity of Delft3D river models to bathymetric variability. The purpose is to increase understanding of river flow characteristics to improve model output. Instruments were deployed in various flow depths and velocities to investigate the effect of these variables on the purported length scales of coherent flow structures. This study considers coherent motions as periodic structures resembling a wave packet, similar to Adrian's (2007) eddy packet description, that propagate in the stream-wise direction and applies Fourier based methods for isolating motions within the flow. The capability of an Acoustic Doppler Current Profiler (ADCP) oriented with a horizontal beam in the stream-wise direction is evaluated to non-intrusively measure flow velocities at large distances. An Iterative Maximum Likelihood Estimator (IMLE) method is used that can resolve length scales up to two or four times the maximum array length, which has not been previously used in riverine environments. The results will show that the resolution of data analysis techniques is an important factor in providing accurate delineation of the motions, and thus length scales, present in the flow.

THIS PAGE INTENTIONALLY LEFT BLANK

II. EXPERIMENT DESIGN

A. EXPERIMENT SITE DESCRIPTION

River velocities were acquired by three different sensors as part of an 8-day riverine field experiment conducted in August 2010 on a braided reach of the Kootenai River near Bonners Ferry, Idaho. The Kootenai River flows south from its headwaters in the Rocky, Salish, and Purcell Mountain ranges through northwestern Montana, turns north and flows through the Kootenai valley of northern Idaho, and reaches its terminus at Kootenay Lake in British Columbia, Canada. The discharge of the Kootenai River is primarily controlled by the Libby Dam in Montana and was a constant 196 m^3/s during the experiment (U.S. Geological Survey 2010). The experiment site is located on two relatively straight 120 *m* wide sections of the main river channel and a narrower 20 *m* wide straight side channel (Figure 1). Bed substrate ranged from coarse gravel to cobbles with particle-size diameters between 20.8 and 78.2 *mm* (D_{16} and D_{84}), with a median particle size (D_{50}) of 39.9 *mm*, where D_x represents the diameter of the *x*th percentile from the bed particle distribution (Fosness and Williams 2009). The river bank is comprised of rough gravel and is approximately 3 *m* wide followed by a steep 6 *m* elevation rise to the floodplain.

The site is divided into four distinct zones characterized by river feature and flow pattern (Figure 2). Zone 1 encompasses a section of the main channel with a thalweg depth >1 *m* and mean flow velocity >1.6 *m/s*. Zone 2 has similar flow characteristics as Zone 1 and is located 2 *km* upstream. Zone 3 includes the 20 *m* wide side channel with a thalweg depth of 1.6 *m* and mean flow velocity of 0.5 *m/s*. The channel narrows and shallows to 0.7 *m* at a 50 *m* long riffle section causing the flow to increase to 1.4 *m/s*. Zone 4 is located downstream of a man-made concrete piling 100 *m* upstream of Zone 3 with a mean depth and velocity of 1 *m* and 0.4 *m/s*. Downstream of the structure, the flow splits at a gravel bar and either continues through to the side channel or re-joins the main channel, where the confluence affects the flow pattern of

Zone 1 near a large gravel bar. Zones 1 and 2 are representative of typical river flows and Zones 3 and 4 contain areas of visible vortex shedding.

B. INSTRUMENTATION

A synchronous lagged array scheme was implemented to compute the expected stream-wise length scales of coherent flow. Stream-wise velocities were measured using a non-equidistant lagged array of six Valeport electromagnetic current meters (ECM), a custom 2 *MHz* Nortek ADCP, and a Nortek Acoustic Doppler Velocimeter (ADV) mounted on a GPS-equipped portable aluminum frame (Figure 3). The frame was designed to support the 4 *m* long ECM array, oriented in the stream-wise direction, and to minimize flow disturbances. The frame was constructed of 5 *cm* diameter pipes and resembled a 2 *m* square scaffold. The bracing and legs were adjustable to locate and level the frame in a variety of river bottom contours. The spacing between each 6.5 *mm* diameter ECM was set to maximize the resolution of coherent motions from 0.5 *m* up to 8 *m* in length using an IMLE method described later. The ADCP was fitted with a custom head (Appendix A) that uses one horizontal, 1.7 degree beam width to measure along beam velocities in the stream-wise direction at equal 35 *cm* bins, up to 10 *m* in length, with a sampling frequency of 1 *Hz.* The stream-wise oriented beam conveniently serves as a high-resolution, equidistant lagged instrument array without the limitations of typical synchronous arrays, such as cabling, a large frame, and a separate data logger. To date, this is the first experiment to use an ADCP to compute scales of coherent flow structures. Since ADCPs are inherently noisy instruments, and the performance of ADVs and ECMs in measuring velocities in turbulent flows (~1.5 *m/s*) has been shown suitable for describing flow characteristics (MacVicar et al. 2007), ADCP velocities are compared to the ECM and ADV (Appendix A).

Stream-wise velocities were measured for a minimum of 1.5 hours at each site. The ADCP and ADV were mounted approximately 1.5 *m* apart in the across-stream direction on the front of the aluminum frame and all sensor heads were placed at approximately mid-depth (Figure 3). The frame was deployed in several locations of the river (Figure 1 and Table 1) that included the large, fast flow main channel, the

smaller, slower flow side channel, downstream of man-made structures, and upstream and downstream of riffles. The scheme for instrument deployment was systematic for Zones 1, 2 and 3, starting near the river bank at approximately 0.5 *m* depth and progressively moving to faster and deeper flows farther out towards mid-channel. In Zones 1 and 2, however, the strong stream-wise current (~1.6 *m/s*) near mid-channel almost caused the instrument frame to topple and prevented velocity measurements for depths greater than 1 *m* for these areas of the river. The slower velocities in Zones 3 and 4 did not limit frame deployments in depths up to 1.5 *m*.

C. DATA VALIDATION

Initial data verification of the first deployment showed that the ECM array measurements were affected by electromagnetic interference from overhead power lines and these datasets were removed from analysis. The ECM array was then deployed farther upstream away from interference in Zone 2 for two days to provide a benchmark for ADCP validation (Appendix A). The larger number of ADCP datasets and longer beam lengths, compared to the ECM array, made these measurements ideal for use in all lagged array analysis methods in this study. Several other datasets were not included in the analysis due to instrument orientation where either the effective beam length of the ADCP was too short for analysis, or river features, such as riffles, prevented accurate coherent flow structure identification. In all, measurements from 10 of the initial 19 deployment locations were used for analysis. A three standard deviation filter to remove outliers was applied to the data (Emery and Thomson 2001). For all ADCP datasets, the mean velocity and energy spectra per bin were plotted to identify the maximum bin where the mean velocity and spectral curve deviated more than 10% from the prior bin's measurement.

THIS PAGE INTENTIONALLY LEFT BLANK

III. DATA ANALYSIS METHODS AND RESULTS

A. SPECTRAL ANALYSIS

Spectra were calculated by dividing the 1.5-hour velocity time series into 20 Hanning windowed subseries of 256 *s* with 50% overlap, resulting in a frequency resolution of 0.0039 *Hz* and 106 degrees of freedom. The process to determine ideal record and subseries length is explained in Appendix B. Longer (>3 hours) ADCP records at fixed locations were divided into several 1.5-hour record lengths providing 15 datasets for analysis. The energy spectra are qualitatively separated into frequency bands and used to compute the respective scales. The average period for the motions in each frequency band is computed by

$$T = \frac{\int_{f_1}^{f_2} E(f)df}{\int_{f_1}^{f_2} fE(f)df}, \tag{2}$$

where E is the energy density and f is the frequency.

Spectral estimates of representative deployment locations for each zone are shown in Figure 4. The spectra consistently show energy in the lower frequencies with a well-defined energy cascade occurring between ~0.02 to 0.1 *Hz*. A noise floor is evident and consistent in all spectra with an amplitude between 0.01 to 0.02 $(m/s)^2$-*s*. Zone 3 and 4 spectra show distinct and significant peaks at 0.01 *Hz* indicating the presence of a strongly periodic motion and is attributed to the formation of vortices that are shed from the riffle (Zone 3) and the man-made concrete piling (Zone 4). Horizontal eddies were visually observed downstream from these features and along the high-speed jet of fluid ejected from the riffle. Application of Taylor's hypothesis (Eq. 1) to the low-frequency periodic motions in Zones 3 and 4 results in a temporal and length scale of 100 *s* and 44 to 53 *m*, however, it is unclear whether the motion applies to the horizontal eddies, vertical flow structures, or their combination. An anomalous spectral peak (not shown) was apparent in a Zone 2 deployment, which had a nearly 5 hour total record length and was divided into three smaller 1.5-hour record lengths.

This anomaly prompted an investigation and test into smaller record lengths (Appendix B), and the test revealed motions that appear periodic in the spectra from record lengths shorter than 1.5 hours are not significantly different than random noise. Since the peaks in Zones 3 and 4 are from energy spectra computed with 1.5-hour ADCP record lengths, the motions are considered significant. An energy roll-off towards zero is not apparent in the lowest frequency bin in Zones 1 and 2. Similar results were obtained by varying the subseries record lengths to increase low-frequency resolution (Figure 5). This suggests that longer record lengths (> 1.5 hours) are needed to increase low-frequency resolution while maintaining statistical confidence. In many cases, the lowest frequency bin approaches zero, but the increased resolution masks any apparent energy cascade and separation of motions is difficult. An accurate temporal scale for the low-frequency motions in Zones 1 and 2 cannot be adequately determined from Eq. 2 without complete frequency limits.

Normalized logarithmic spectra for each ADV deployment were plotted together (Figure 6) and linear regression used to compute slopes associated with the features visible in the spectra. The motions in the low-frequency band (< 0.05 *Hz*) have a mean slope near zero suggesting the presence of large-scale, low-frequency structures. The roll-off, or cascade, of energy in the ~0.02 to 0.1 *Hz* frequency band is typical of turbulent motions, but the mean slope of -1 differs from the expected -5/3 slope associated with turbulence. Similar spectral slopes were noted in a laboratory experiment on turbulent river flows conducted by Carrasco and Vionnet (2004). This suggests the presence of an inverse energy cascade, where energy is transferred to the low-frequency motions from higher frequency turbulence. An energy cascade, or spectral gap, usually determines the separation of motions present in the flow (Carrasco and Vionnet 2004; Vickers and Mahrt 2003) and based on experiments by others (e.g., Sukhodolov and Uijttewaal 2010), the energy cascade represents turbulence within the flow and separates the low-frequency, energetic motions from the noise floor. The frequency band of turbulence is qualitatively determined and noted as an upper limit for the low-frequency motions. The limit ranges between 0.0078 to 0.0625 *Hz* and is consistent for all datasets of the same deployment. Roy et al. (2004) noted a frequency

band of 0.07 to 0.12 *Hz* for coherent flow structures in a relatively slow, shallow flow (0.67 *m/s* and 0.32 *m*). They used a 20 *min* total record length divided into 60 *s* subseries lengths. Their choice of window length is described in Buffin-Belanger and Roy (2005) in which the low-frequency spectra contained <3 % of the total signal energy (variance), and therefore, in their study, the record lengths could be truncated to disregard the low-frequency motions.

Normalized cumulative integrated spectra were computed, which represents the percentage contribution of the motions to the total variance per frequency (Figure 7). Disregarding the noise floor ($f > 0.25$ *Hz*), the spectra show that between 40 to 50% of the variance is contained in the low-frequency (<0.05 *Hz*) band prior to the energy cascade. This result indicates that the low-frequency motions in this study are significant and cannot be ignored.

B. COHERENCY

Signal coherency is a Fourier based method to measure the linear correlation by frequency of two signals acquired by two sensors with spatial separation. Two time series are transformed into the frequency domain through Fourier techniques and compared to determine if the signals are coherent as a function of frequency (Emery and Thomson 2001). The squared coherency function between two sensors is defined as

$$\gamma_{1,2}^2(f) = \frac{\left|C_{1,2}^2(f) + Q_{1,2}^2(f)\right|}{\left|S_{1,1}(f)\right|\left|S_{2,2}(f)\right|}, \tag{3}$$

where $\left|S_{1,1}(f)\right|$ and $\left|S_{2,2}(f)\right|$ are the auto-spectra of the two signals, $\left|C_{1,2}^2(f)\right|$ and $\left|Q_{1,2}^2(f)\right|$ are the co-spectrum and quadrature spectrum of the cross-spectrum, and $0 \le \left|\gamma_{1,2}^2(f)\right| \le 1$. Two completely correlated signals, without noise, will have a γ^2 equal to 1 while two un-correlated signals will have a γ^2 equal to 0. A γ^2 between 0 and 1 occurs if either the signals are not linearly related or noise is contained within the measurements (Bendant and Piersol 2000). Confidence limits for γ^2 are specified to

delineate a significance level threshold at which point the signals are no longer statistically similar. A significance level of 0.06 is obtained for a confidence level of 95% from a chi-square distribution with 106 degrees of freedom (Emery and Thomson 2001). Therefore, two velocity signals are considered coherent if γ^2 is between 0.06 and 1. The maximum sensor separation that retains coherency, as a function of frequency, is the coherent length (L_c) of the signal. L_c indicates the distance at which the signal is statistically the same or, in other words, the distance that the signal persists before it can no longer be considered the same signal. The L_c of a signal is not an indication of its total motion length, as a signal can persist longer or shorter than its length. The coherence time (T_c), which is the persistence time of a coherent signal, is calculated from L_c by

$$T_c = \frac{L_c}{U}, \tag{4}$$

assuming Taylor's hypothesis. This technique is used to confirm the presence of coherent motions, as a function of frequency, and to provide L_c and T_c of the large scale motions.

Stream-wise velocity coherency was computed at the first ADCP bin relative to each successive bin up to the maximum beam length (Figure 8 a–b). Coherency decreases to lower frequencies with increasing lag suggesting larger L_c for the low-frequency motions. The maximum lag at which coherency is retained ($\gamma^2 > 0.06$) is determined and plotted as a function of frequency (Figure 9). The maximum distance is long for low frequencies and decreases rapidly for higher frequencies. A triangular plot marker is used to indicate the instances when the maximum lag at which coherency occurs equals the maximum bin size. L_c for the low-frequency motions are longer than the beam lengths of the representative flows measured in each zone (Figure 9). In Zones 1 and 3, the low-frequency coherent motions persist farther than 6 to 9 *m*. The mean γ^2 for the energetic, low-frequency band motions in Zones 1 and 2 and γ^2 (f = 0.01 *Hz*) for Zones 3 and 4 appear to linearly decrease as a function of bin lag (Figure 10). A linear best-fit line suggests the low-frequency coherent motions persist up to 10 *m* (Zones 1 and 2) and 22 to 27 *m* (Zones 3 and 4). Linearly extracted L_c, with

corresponding T_c and L_c/h values are listed in Table 2. Low-frequency energetic motions are at least temporally coherent, have relatively long L_c, and therefore, this study considers these motions as large-scale coherent flow structures.

C. FREQUENCY-WAVENUMBER ANALYSIS

Next, the stream-wise spatial scales for the coherent flow structure are extracted from frequency-wavenumber (f-k_s) spectral analysis. This method has been used extensively in nearshore experiments to compute long, infragravity wave energy as a function of frequency and wavenumber (Pawka 1983; Oltman-Shay and Guza 1987; Oltman-Shay et al. 1989; Reniers et al. 2006). These periodic waves have temporal and spatial scales of 20 to 200 *s* and 20 to 1000 *m* (Oltman-Shay and Guza 1987). The wavenumber (inverse length), **k**, is a vector comprised of an across-stream component (k_a) and a stream-wise component (k_s). Lagged sensor arrays are usually deployed, and f-k_s spectra for each frequency are computed for propagating wave components (Capon 1969). The f-k_s spectra are determined from the spatially lagged cross-spectrum $[M(\ell, f)]$ by

$$E(f, k_s) = \int M(\ell, f) \exp(-ik_s \bullet \ell) d\ell , \tag{5}$$

where $E(f,k_s)$ is the spectral value at frequency f and stream-wise wavenumber k_s and ℓ is the spatial lag. The complex cross-spectrum is determined by Fourier decomposition according to

$$M_{ij}(f) = F_f\{v(s_i, t)\} F_f^*\{v(s_j, t)\}, \tag{6}$$

where $F_f\{\ \ \}$ is the complex Fourier coefficient at frequency, f, of the velocity component, v, at the stream-wise locations s_i and s_j. Two-dimensional Fourier decomposition to produce the cross-spectrum matrix $[M_{ij}(f)]$ can only be computed at the discrete equal lag separations of the sensors in the array which yields low resolution results for $E(f,k_s)$ (Sheremet et al. 2005).

If the motion lengths of interest are longer than the array length or the instrument array consists of unequally spaced lags, high-resolution estimation methods

can be used (Oltman-Shay and Guza 1987). An IMLE method provides a linear estimator of $E(f,k_s)$ and has the form

$$\hat{E}(f,k_s) = \sum_i \sum_j \alpha_{ij}(f,k_s) M_{ij}(f), \tag{7}$$

where $\alpha_{ij}(f,k_s)$ are complex variable weights composed of sines and cosines (Pawka 1983). The cross-spectra are computed at each frequency, then IMLE applies a best-fit curve algorithm to the spectra, and k_s values are extracted from the curve fit. This curve fit is optimal when at least two points of the passing wave are captured in the cross-spectrum. Tests performed by Oltman-Shay and Guza (1984) show the IMLE method provides the most accurate estimate of the energy contained per wavenumber bandwidth, and total energy estimates were accurate to within 1% of the true spectrum. IMLE extends the array by extrapolating the measurements and increases the wavenumber resolution up to four times the array length with more statistically confident estimates at twice the array length (Sheremet et al. 2005). The co-spectra for various frequencies of a Zone 2 deployment are shown in Figure 11 to emphasize the IMLE process. In the low frequencies (<0.063 *Hz*), less than a half motion length is computed and therefore, wavenumbers cannot be confirmed below this frequency. The co-spectra at a higher frequency (0.49 Hz) reveal that the motions decay at longer lags. This is a common result of this technique (e.g., Oltman-Shay et al. 1989, Figure 5) and is similar to the results of coherency analysis, since both techniques use co-spectra computations in their formulations. The IMLE method is used to compute the estimated f-k_s spectra for the stream-wise velocities (Figure 12).

A length scale is obtained from

$$L = \frac{\int_{k_{s_1}}^{k_{s_2}} \int_{f_1}^{f_2} E(f,k_s)\,df\,dk_s}{\int_{k_{s_1}}^{k_{s_2}} k_s \int_{f_1}^{f_2} E(f,k_s)\,df\,dk_s}, \tag{8}$$

where k_{s_1} is the wavenumber limit determined by two or four times the maximum array length and k_{s_2} is the Nyquist wavenumber determined by

$$k_{s_2} = \frac{1}{2\Delta\ell}, \tag{9}$$

where $\Delta\ell$ is the smallest instrument lag separation in the array. The wavenumber limit, k_{s_1}, determines the resolvable limit of f_1. Wavenumbers computed by doubling the array length provide statistically conservative estimates, while those computed with four times the array still provide reliable, but less confident, estimates. Length scales are obtained by averaging the wavenumbers over the frequency bands (f_1–f_2) identified from energy spectra that separate the low-frequency, coherent flow structures and turbulence.

A ridge of energy as a function of f-k_s follows the advective velocity of the flow according to Taylor's hypothesis (Eq. 1), highlighted in Figure 12. The f-k_s spectra show concentrations of energy in low-frequency, small wavenumber (large motion length) bands suggesting the coherent flow structures have relatively long periods and lengths. The spectra reveal that the wavenumbers for the low-frequency, coherent flow structures are beyond the resolvable range of the array length. In the spectra of a Zone 3 deployment, with a beam length of 9 *m*, a small frequency band of the coherent flow structure was available to extract a length of around 7 *m* (Table 3). The actual mean structure length should be much larger and could be confirmed if the ADCP beam length was longer, but nevertheless, this short structure length is larger than the predicted 2 to 6*h* scale. Mean motion lengths, *L*, averaged over the turbulence frequency band, are computed from Eq. 8 for each dataset (Table 3). In some datasets, indicated by an asterisk in Table 3, the array length prevented the determination of the full range of motion lengths for the turbulence. The actual lengths for the low-frequency, coherent flow structures are much larger than anticipated, highlighting the need for a longer (>> 10 *m*) array length.

D. MULTI-RESOLUTION DECOMPOSITION

To address the resolution of a lower frequency limit for the coherent flow structures, multi-resolution decomposition (MR) has been used in analyzing turbulent fluxes and provides coarse time-scales of fluctuations, or events (Vickers and Mahrt 2003). MR is a type of spectral averaging, which computes sample variance associated with 2^P averaging length time-scales and represents the simplest orthogonal

decomposition (Vickers and Mahrt 2003). Howell and Mahrt (1997) describe the spectra produced from MR as simultaneous decomposition of a signal into un-weighted moving averaging windows of different widths. Both Fourier methods and MR preserve signal variance, but unlike Fourier where the spectral peak in the frequency domain depends on periodicity, the peak of MR spectra in the time domain depends on time-scale fluctuations in the signal (Vickers and Mahrt 2003). A complete explanation of MR is given in Howell and Mahrt (1997) and a brief description of the MATLAB software algorithm provided by Vickers (2010, personal communication) is presented herein. Given a time series of 2^P data points, MR first partitions the record into simple averages of different segments of width 1, 2, 4…2^P points. The segments are sequenced as $n = 2^P, 2^{P-1}…1$, where n is the position of the segment within the series. The averages are removed from each consecutive sub-segment starting with the largest scale (2^P width) and ending with the shortest time-scale. The average for the nth segment of scale p is given by

$$\bar{v}_n(p) = \frac{1}{2^p} \sum_{i=(n-1)2^p+1}^{n2^p} vr_i(p), \tag{10}$$

where $vr_i(p)$ is the residual series after segment averages with windows of width > 2^p points are removed. The process starts with the largest segment (the entire time series) and removes the mean from all the data points. The resulting time series is the 1st residual series. The next step moves to the next smaller segment, which is half the length of the original time series and composed of 1st residual series values and removes the segment mean from the respective segment data points resulting in the 2nd residual series. The process continues to remove the segment means from each segment as it proceeds through to the shortest time-scale associated with the record length. The average for each nth segment is used to calculate the MR spectra, which represents the variance of the segment averages and is given by

$$D_v(p+1) = \frac{1}{2^{P-p}} \sum_{n=1}^{2^{P-p}} \bar{v}_n^2(p), \tag{11}$$

where $v_n(p)$ is the segmented, mean removed time series, $D_v(p+1)$ is the variance of $v_{(n-1)2^{p+1}}$ associated with an averaging time scale of 2^{p+1} data points, and the sum of

$D_v(p+1)$ is the total signal variance. The MR spectra have units of variance as a function of averaging time-scales from which upper and lower time-scale limits can be obtained and converted to coarse frequency scales. An example of the MR response to a synthetic periodic time series signal and resulting test spectra is shown in Appendix C. The test revealed MR limitations that affect the resolution of the frequency boundaries, such that MR only provides coarse limits for the frequencies of the motions.

The averaged MR spectra for each zone are shown in Figure 13. The 32 *Hz* sampling rate of the ADV allows defining the higher frequency limit of the MR analysis. From the test spectra in Appendix C, the peak in the MR spectrum corresponds to the frequency that captures the higher frequency limit of the signal variance or energy. The MR spectra of the ADV stream-wise velocities consistently have peaks at 0.125 *Hz*. To the left of the MR spectra peaks, the variance steadily decreases and where the spectra levels out to the lowest frequency, or approaches zero, indicates the lower frequency limit. This limit consistently occurs at 0.001 *Hz*. The periods, *T*, of the coherent flow structures were computed using Eq. 2 where f_1 is 0.0039 *Hz* and f_2 is determined from energy spectra. Table 4 lists the variables *T*, *L*, and *L/h* for each dataset, where *L* is the coherent flow structure length determined from Eq. 1. The length scales range from 25 to 91 *m*, however, care must be exercised when interpreting the scales of motion determined from this method. The low-frequency limit is an *in extremis* boundary, that is, the signal contains no motion less than 0.001 *Hz*, but the actual limit is between 0.001 and 0.0039 *Hz*. Choosing an incorrect frequency limit will skew the mean *T*, and therefore, the lengths in Table 3 represent another coarse resolution description of the possible lengths for coherent flow structures.

THIS PAGE INTENTIONALLY LEFT BLANK

IV. DISCUSSION

The results provide an indication of the potential length scales of large-scale coherent flow structures in a deeper and faster gravel-bed river than previously measured in the field. Energetic, low-frequency motions containing 40 to 50% of the spectral energy were found for all deployment locations. The low-frequency motions are identified as large-scale coherent flow structures as measured by their relatively long coherent length-scale. L_c for the low-frequency structures, which averaged 25 *m* in the slower flows and 10 *m* in the faster flows (Table 2), were shorter than their corresponding motion lengths (Table 3). This implies the flow structures are not coherent for their entire length, and suggests the structures evolve as they propagate downstream that is shown in Figure 10 as a decrease in coherency with lag.

Decay in coherence is caused by either a change in amplitude or a shift in period as the structure passes through the array (Bendant and Piersol 2000), and appears to occur more rapidly in the faster, more turbulent flows. There are several possibilities responsible for this process. A change in period, or frequency shift, may be the result of an energy transfer between scales of motions as noted by Carrasco and Vionnet (2004) in a turbulent flow experiment. If the coherent flow structures are considered alternating regions of high and low-speed wedges as described by Roy et al. (2004), L_c may correspond to a single wedge. The succeeding wedge would then appear as a structure with different frequency or amplitude.

Dinehart (1999) discussed the potential of a group of high-speed pulses appearing as low-frequency motions, which can result from Fourier analysis creating an apparent period. For example, IMLE predicted wavenumbers are based on fitting periodic functions to the velocity co-spectra, and therefore, the method "forces" the results to be periodic. The results from f-k_s indicate that the ADCP beam length was not long enough to reliably capture either the motion lengths or the coherent lengths of the low-frequency flow structures. A longer (> 20 *m*) beam length is needed to capture these flows. This substantial sized array explains why most studies have been confined

to slow, shallow flows requiring shorter arrays and questions the validity of a 2 to 6h length scale for fast, deep flows. A longer array will only confirm the linearly extrapolated values for L_c, but longer motion lengths may still remain unresolved.

V. SUMMARY AND CONCLUSIONS

This study was motivated by Dinehart's (1999) observation of large coherent flow structures in a relatively fast and deep gravel-bed river that did not fall within a 2 to 6*h* length scale. Several days of stream-wise river velocity measurements were examined in a braided reach section of the Kootenai River, ID with the objective of determining a characteristic length scale for large coherent flow structures. A custom ADCP head was validated for use as a reliable, accurate, and convenient instrument for obtaining stream-wise velocities at relatively long beam lengths with finer spatial resolution and less influence on the flow than a comparable ECM array. In the outer region of river flow, low-frequency coherent structures, or rolling vortices as described by Shvidchenko and Pender (2001), propagate downstream at the advective velocity of the flow according to Taylor's hypothesis as confirmed by f-k_s spectra. The structures have coherent lengths from 5 to 22 *m* (Table 2) and motion lengths that could be as long as 25 to 90 *m* (Table 4). Dinehart (1999) noted similar large scales that were attributed to gravel-bed form migration during storm flow events, neither of which occurred in the flows of this study. Coherency results suggest the structures evolve in either amplitude or period prior to reaching their full-length scale. The specific change of the structures was not determined, but indications are that some mechanism caused the motions to alter their characteristics. Although this study did not provide a precise stream-wise length scale, it succeeded in showing, through spectral techniques unique to river applications, that these structures are relatively large, have long lengths, and are coherent for long distances. The study also shows that a record length longer than 5 hours is required to resolve the low-frequency coherent motions with statistical confidence and an array length of 20 *m* or greater is needed to capture the coherent lengths of large-scale flow structures within the measured flows. In summary, energetic, low-frequency motions were measured in fast and deep flows. These motions are coherent along the length of the array with an L_c determined to be longer than the array. The coherent flow structures are longer than a 2 to 6*h* scale, and the structures persist shorter than their motion lengths. These observations indicate an area

of future research to determine the life cycle of coherent flow structures to increase understanding of their generation and the mechanism that alters their lengths in a relatively short distance.

APPENDIX A: CUSTOM ACOUSTIC DOPPLER CURRENT PROFILER VALIDATION

An increasing number of riverine environment studies have used ADCPs to acquire velocity and depth measurements (Gunawan et al. 2010; Muste et al. 2004). These instruments are relatively inexpensive and easy to use. A typical ADCP uses three angled acoustic beams to measure velocities which pass through a measurement volume at some fixed distance from the instrument head and requires a rotation calculation to convert the measurements into the local coordinate axes. The 2 *MHz* ADCP used herein was fitted with a custom head that uses one horizontal, 1.7 degree beam width to measure along beam velocities in the stream-wise direction at equal 35 *cm* bins, up to 10 *m* in length, with a sampling frequency of 1 *Hz.* The stream-wise oriented beam conveniently serves as a high-resolution, equal-spaced instrument array that is non-intrusive and in a small package, however, ADCPs are inherently noisy instruments. Also, the acoustic beam is susceptible to side-lobe scattering by surface and bottom interaction if the narrow ADCP beam width is not properly aligned in the horizontal. The velocity measurements collected by the rigidly mounted, ADCP head are compared to the ECM array and ADV. Since the ADCP had the lowest sampling frequency, variances were computed from 0.0039 *Hz* to the Nyquist frequency of 0.5 *Hz*. The difference in spectral variances between the ADCP, ADV, and an ECM sensor was consistently less than 10% (e.g., Figure 14). The spectra of the three instruments were equal in amplitude as a function of frequency and are not aliased by the coarse 1 *Hz* sampling frequency. The f-k_s spectra from the ADCP and ECM array also compared well with similar energy and wavenumber estimates (Figure 14). The results validate the ADCP velocity measurements for data analysis and show that the custom ADCP is a reliable and convenient instrument for resolving the scales associated with large coherent flow structures.

THIS PAGE INTENTIONALLY LEFT BLANK

APPENDIX B: ENERGY SPECTRA ESTIMATES

Fourier spectral analysis is explained in detail in most time series analysis texts such as Bendant and Piersol (2000) and Emery and Thomson (2001). To compute energy spectra, averaging is done over a number of windows with a choice of window type. A Hanning tapered window was chosen in this study to reduce spectral leakage and it provides a balance of resolution and statistical confidence (Biltoft and Pardyjak 2009). The relationship between frequency resolution and window length is defined by

$$\Delta f = \frac{1}{T_w}, \tag{B-1}$$

where T_w is the window length. A window length of 256 *s* (Δf =0.0039 *Hz*) was chosen as a compromise between frequency resolution and total record length and follows Sukhodolov and Uijttewaal (2010) recommendation for a window length on the order of a few hundred seconds to minimize standard error and variance losses. Degrees of freedom, which is the number of statistically independent values used in each spectral estimate, is determined for a Hanning window by

$$DOF = \frac{8}{3} \times \frac{T_T}{\left(T_w \diagup 2 \right)}, \tag{B-2}$$

where T_T is the total record length (Emery and Thomson 2001). Energy spectra of each velocity time series asymptote to a common 106 DOF, which denotes the number of windows that captures most of the signal variance (Lesht 1980). The selected parameters result in T_T of ~1.5 hours.

A significant spectral peak was found in the middle record of a longer ADCP dataset (~ 5 hour record length). Despite the process used to establish ideal Fourier analysis parameters just described, a test was conducted to determine if a smaller T_T would be valid for analysis. A Zone 2 dataset was divided into T_T sizes of 10, 20, 30 and 60 *min* (T_w = 256 s) (Figure 15). The spectra of the smaller T_T returned significant peaks suggesting clearly defined periodic motions within the flow. Even though *DOF* were reduced in the smaller T_T , the peaks are significant based on 95% confidence

intervals computed from a chi-square test value (Emery and Thomson 2001). A consistent peak across consecutive spectra does not appear and the frequency band at which a peak occurs is not consistent. A random Gaussian noise signal was generated with the mean and standard deviation (1.4 and 0.23) of the river velocities to test the validity of the peaks and T_T under the premise that any signal can appear periodic, given a small enough T_T. Surprisingly, significant peaks are noted in the noise signal spectra (Figure 16) up to a ~1.5 hour T_T. This result suggests that any significant peaks in energy spectra from a T_T less than 1.5 hours cannot be confidently discernable from random white noise.

APPENDIX C: MULTI-RESOLUTION DECOMPOSITION TEST SPECTRA

A single synthetic periodic signal composed of several low-frequency periodic sub-signals was created to analyze the behavior of MR. The amplitudes of the sub-signals were held constant since no appreciable change was noted in the MR spectra when the amplitudes were varied. The range of frequencies for the synthetic signal was chosen to produce MR spectra similar to field datasets. A spectrum and MR of the synthetic signal is shown in Figure 17. The frequencies of the synthetic sub-signals are plotted on the MR to highlight how the shape of the resulting MR spectrum is used to determine signal frequency limits. The peak in the MR spectrum corresponds to the averaging time-scale, which captures the higher frequency limit of the signal. The MR spectrum decreases from the peak to lower frequencies and the point at which the spectrum levels out or approaches zero denotes the lower frequency limit of the signal. The test revealed MR is limited by a significant amount of spectral leakage associated with the 2^P time-scale separation, and the variance of the motions for a particular time-scale are shifted to the next lower time-scale.

THIS PAGE INTENTIONALLY LEFT BLANK

APPENDIX D: FIGURES AND TABLES

Figure 1. Overview of a section of the Kootenai River, ID and instrument deployments (circles). Separation of deployments into zones is highlighted (boxed areas) and described in Figure 2

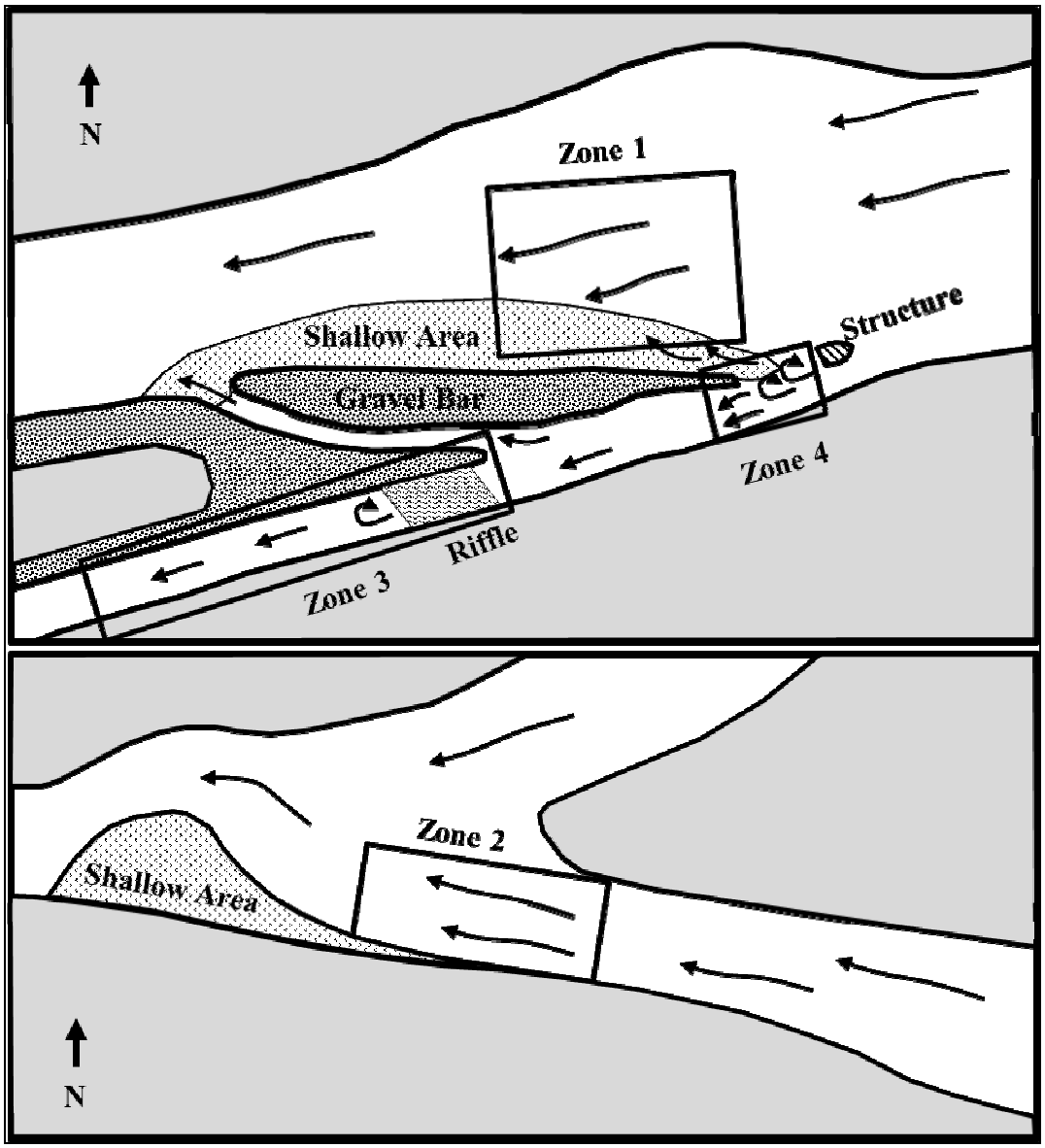

Figure 2. Diagram depicting separation of zones used in this study. Zone 1 encompasses a section of the main channel. Zone 2 is located 2 *km* upstream. Zone 3 includes the side channel, which contains a riffle section. Zone 4 is located downstream of a man-made concrete piling 100 *m* upstream of Zone 3.

Figure 3. Picture of frame with ECM array (not visible), ADV, and ADCP deployed in the Kootenai River, ID.

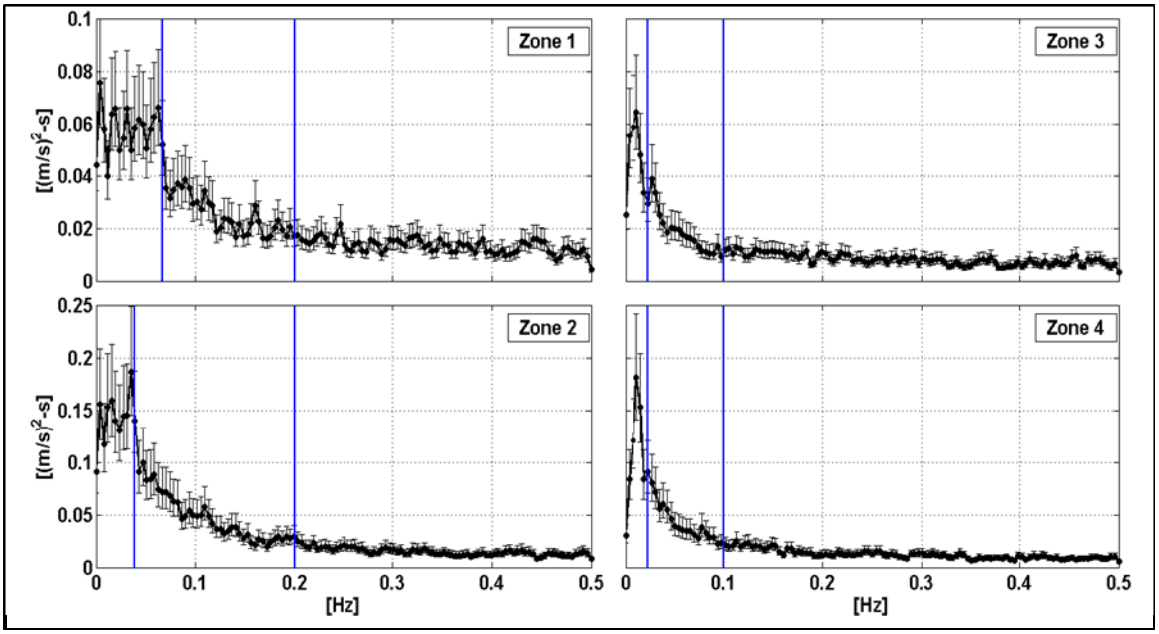

Figure 4. ADCP velocity spectra for representative locations in each zone (Figure 2) with 95% chi-square confidence limits. Separation of motions between the low-frequency energetic structures and turbulent energy cascade is denoted by solid vertical lines.

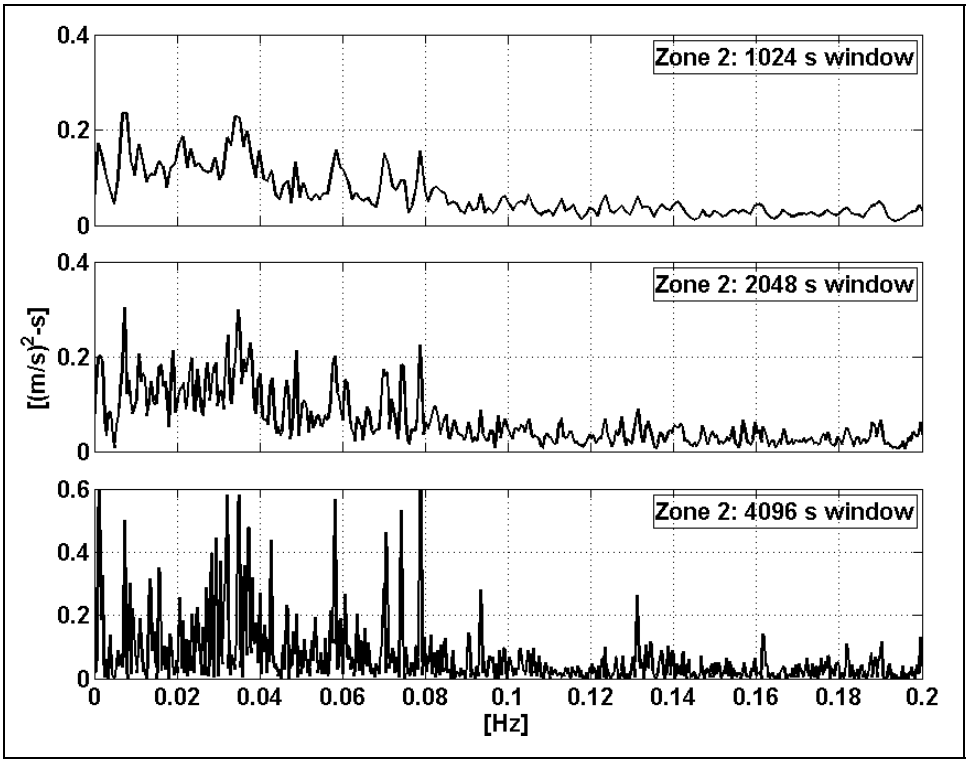

Figure 5. Spectra of Zone 2 (Figure 2) ADCP velocities computed up to the noise frequency limit (0.2 Hz) using varying window lengths up to the total record length (~1.5 hrs).

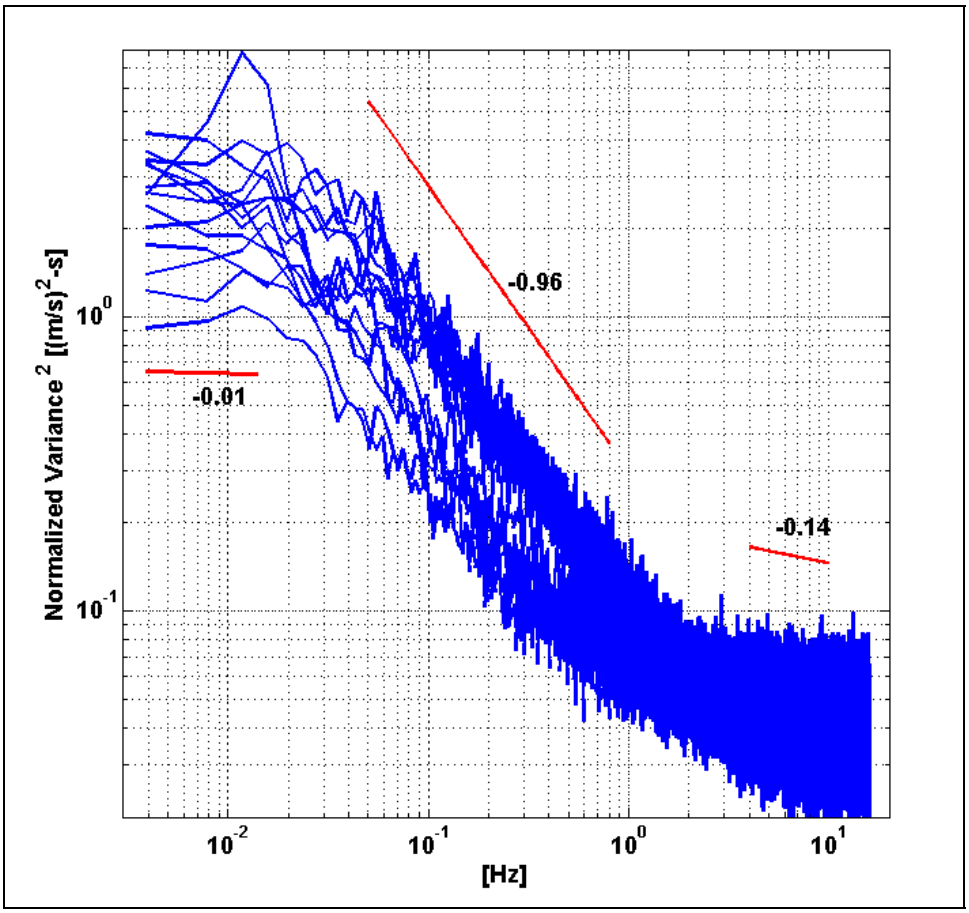

Figure 6. Normalized logarithmic spectra of all ADV deployments with mean slopes of associated motions within the flow (low-frequency motions, mid-frequency turbulence, and high-frequency noise).

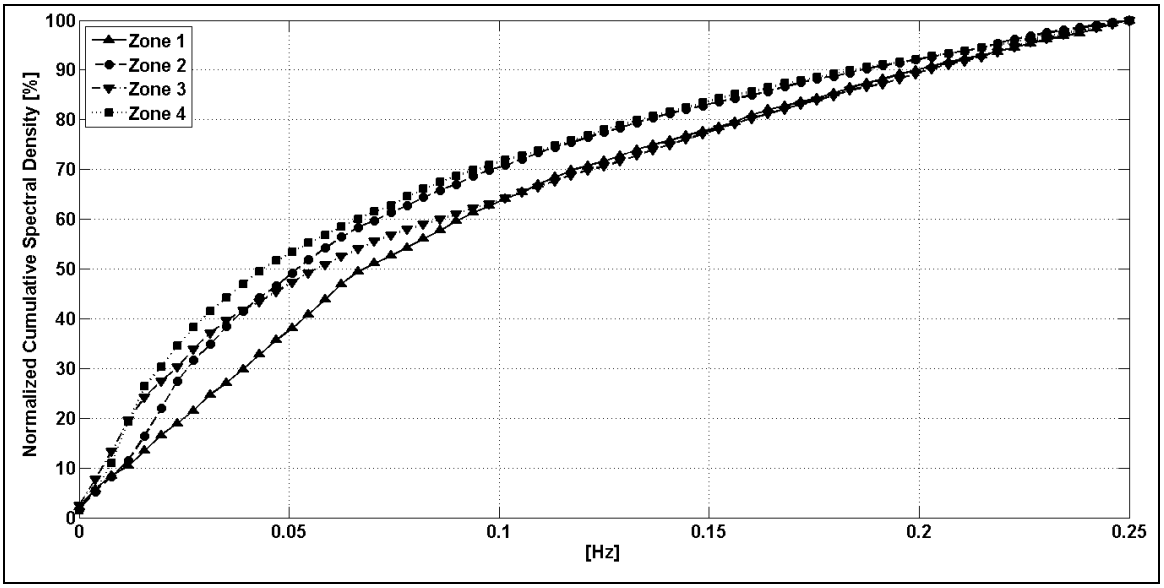

Figure 7. Normalized cumulative spectral density for representative deployments in each zone (Figure 2) denoting the percentage contribution of the motions to the total variance per frequency bin, disregarding the noise floor ($f >$ 0.25 *Hz*).

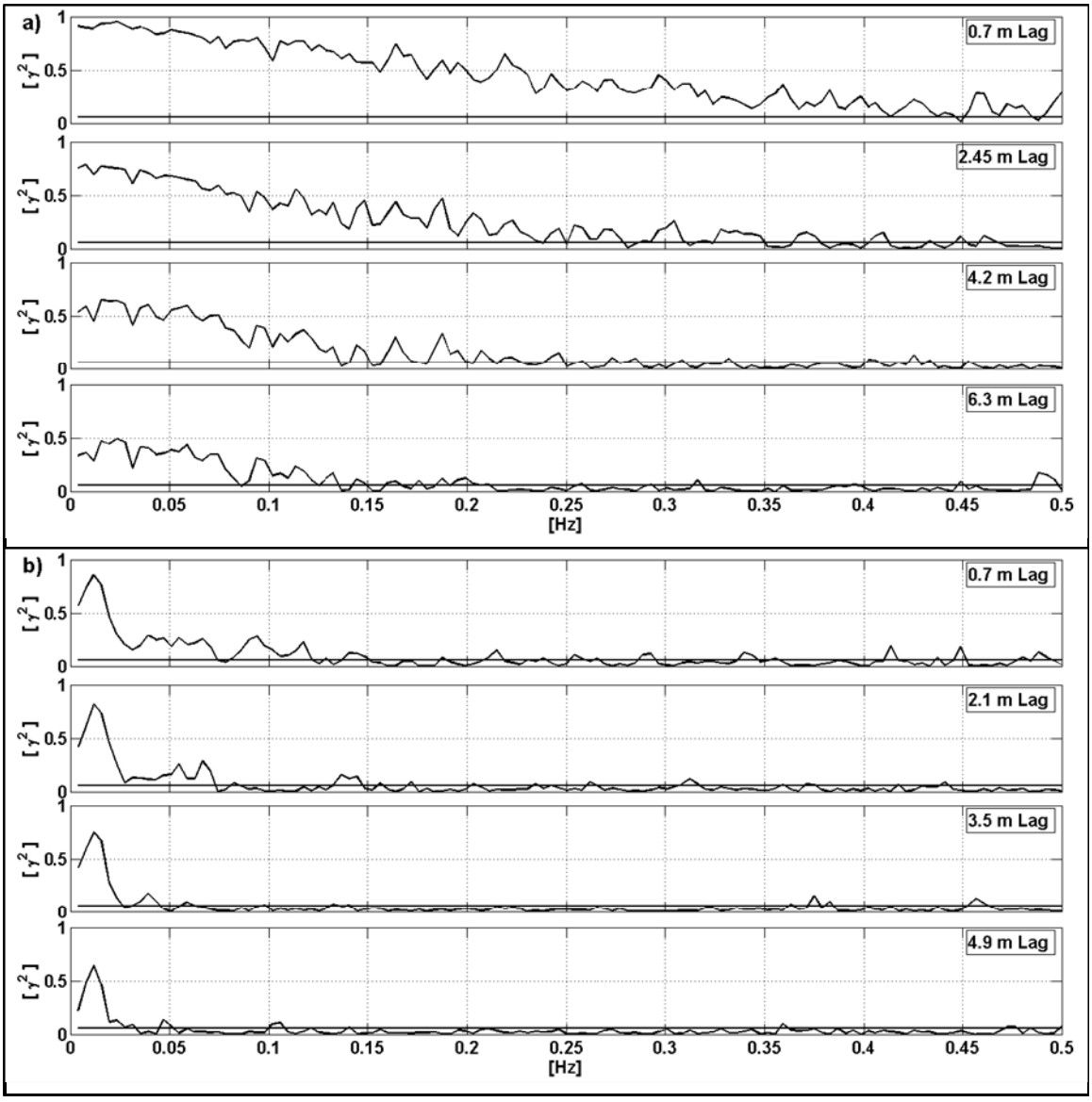

Figure 8. Coherency determined between the velocity measurement at the first bin and the velocity measurement at various lags up to the maximum ADCP beam length for representative deployments for Zone 2 (a) and Zone 4 (b) (Figure 2). Solid horizontal line denotes significance level (0.06).

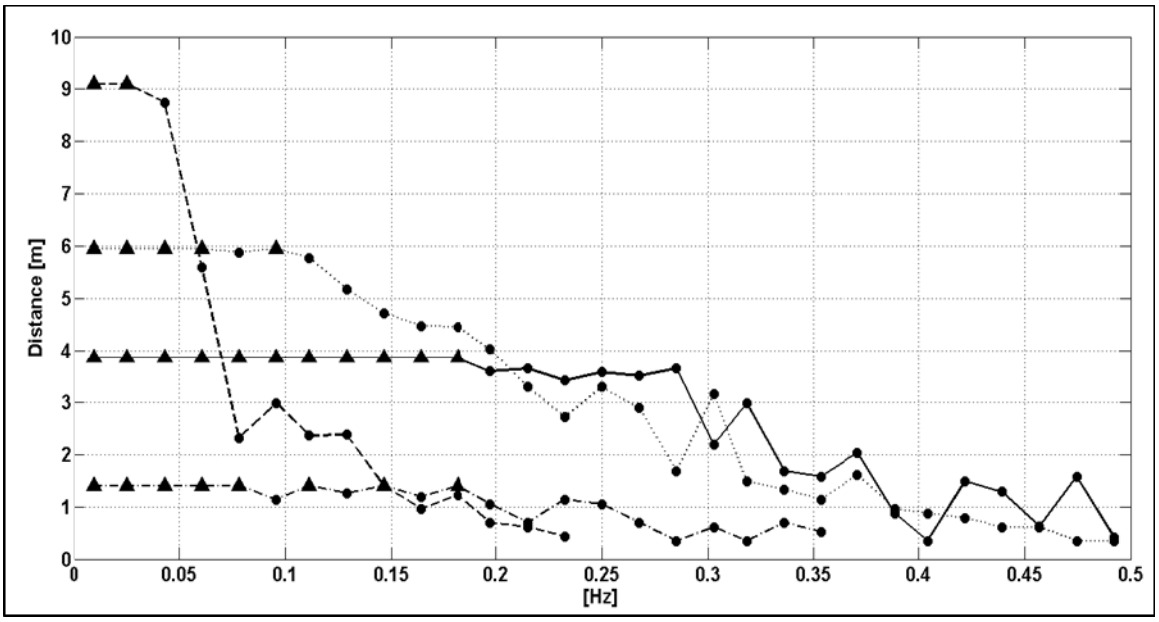

Figure 9. The bin that retains the maximum coherent distance is plotted as a function of frequency for representative deployments of Zone 1 (solid line), Zone 2 (dotted line), Zone 3(dashed line), and Zone 4 (dashed-dot line) (Figure 2). Triangle markers indicate coherence exceeds the maximum ADCP bin distance.

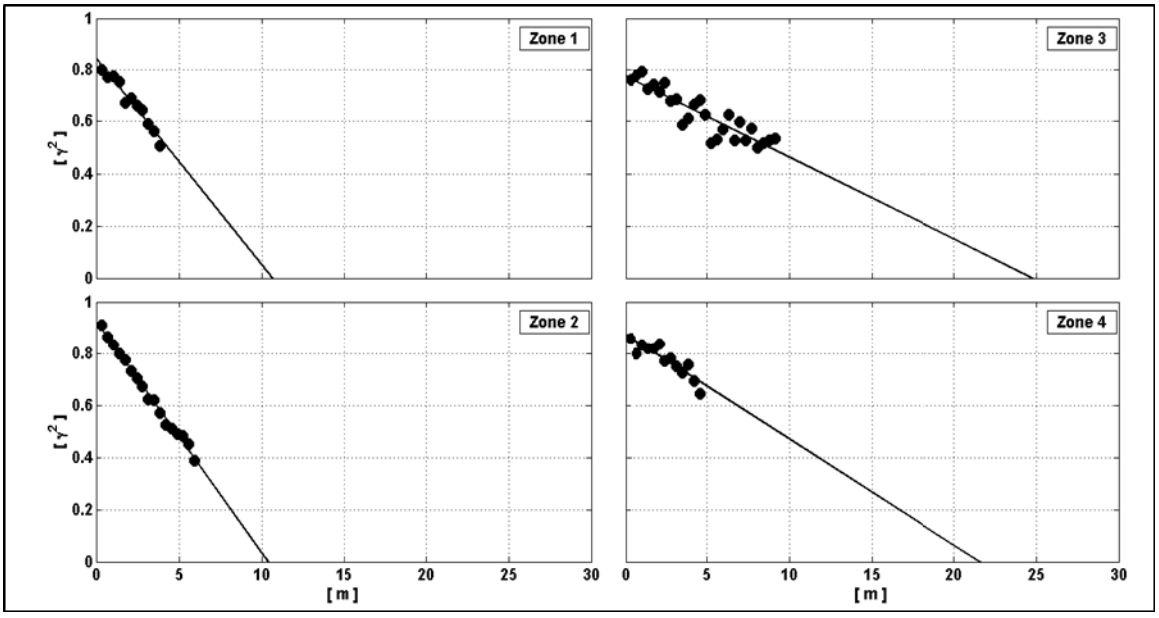

Figure 10. Squared coherency function computed for the frequency band of low-frequency coherent flow structures as a function of ADCP bin lag for representative deployments in each zone (Figure 2). Coherent lengths are extrapolated from the fitted line.

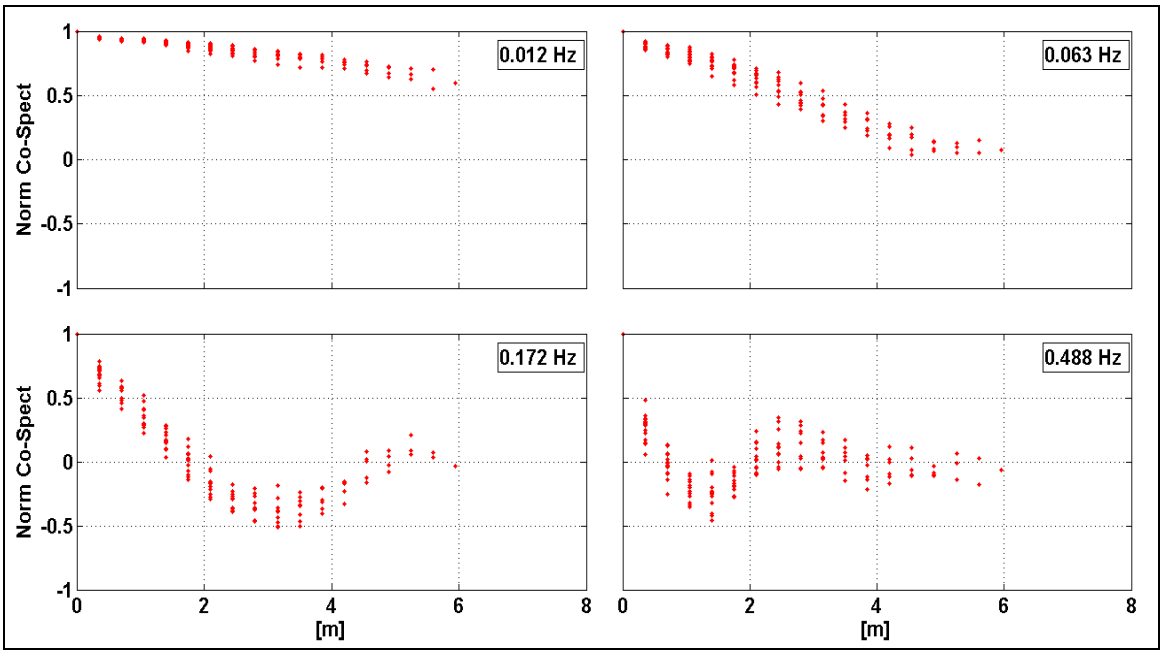

Figure 11. Normalized co-spectra, as a function of bin lag, at various frequencies for ADCP velocities from a Zone 2 deployment (Figure 2).

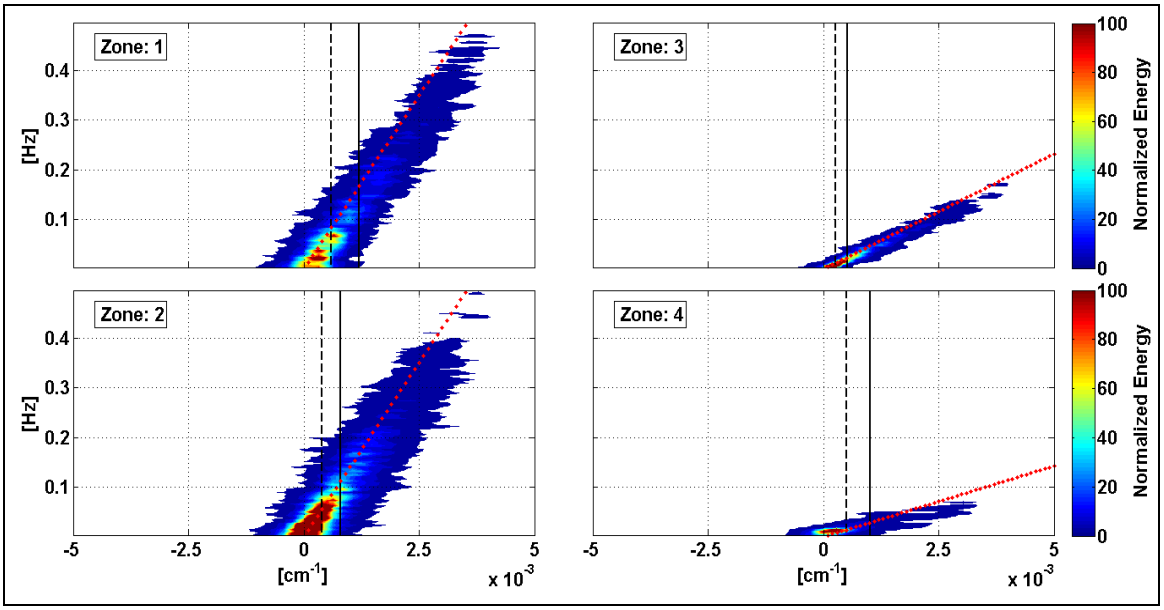

Figure 12. Frequency-wavenumber spectra of velocity time series (ADCP) with associated advective velocity (dotted line) according to Taylor's hypothesis (Eq. 1) for representative deployments in each zone (Figure 2). Vertical lines represent the theoretical maximum motion length resolution of f-k_s as either two (solid) or four times (dashed) the ADCP beam length.

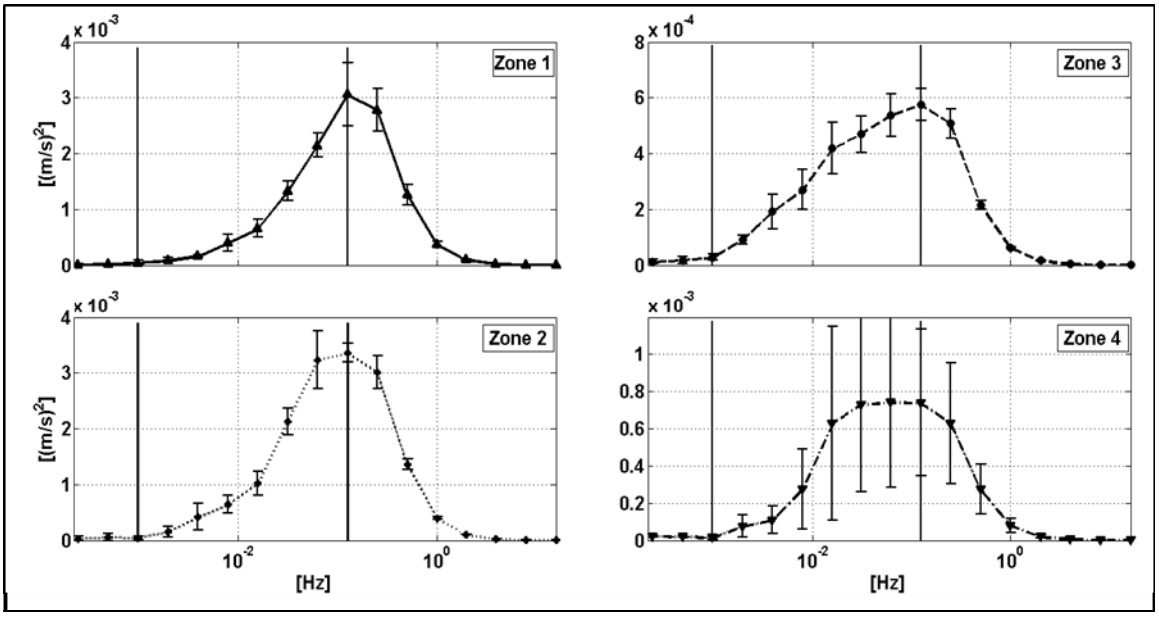

Figure 13. Multi-resolution decomposition of the stream-wise ADV velocities. MR spectra for each deployment are averaged for each of the zones (Figure 2) with standard deviation error bars. Vertical lines denote frequency limits of the signals.

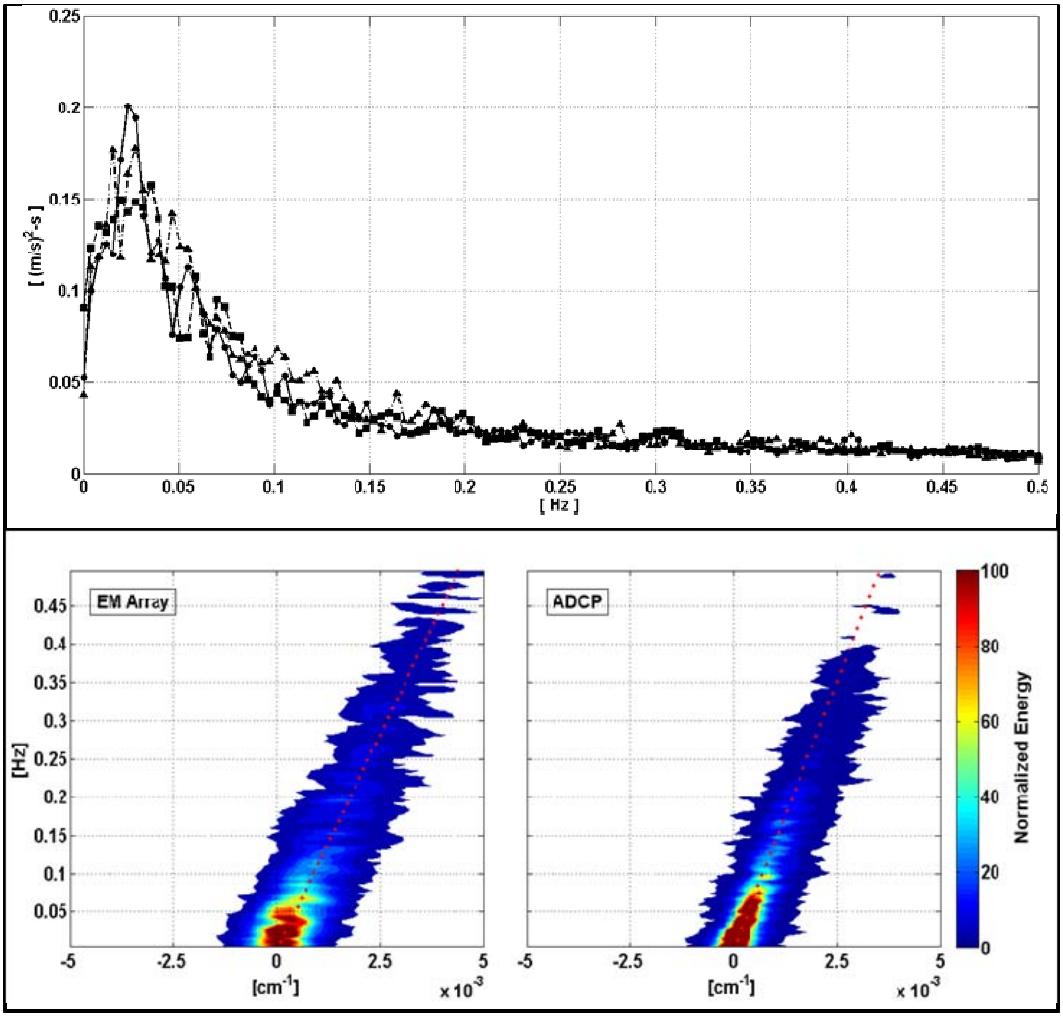

Figure 14. Spectra (top) of ECM (circles), ADV (triangle), ADCP (square) velocity measurements and f-k_s spectra (bottom) for a Zone 2 deployment (Figure 2). Spectral variances are computed up to the ADCP Nyquist frequency (0.5 *Hz*). Differences of variance between the ADCP (0.0179 m^2/s^2) and the ECM (0.0180 m^2/s^2) and ADV (0.0195 m^2/s^2) were computed as 0.78% and 8.6%. F-k_s spectra (bottom) of ECM and ADCP array compared well.

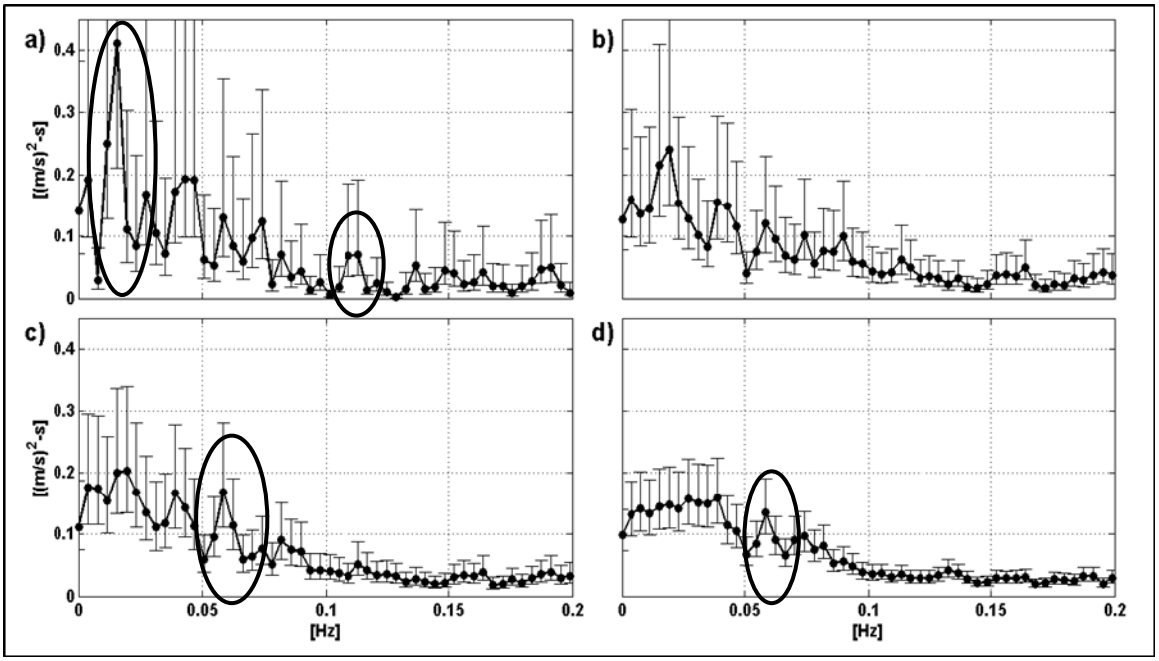

Figure 15. ADCP velocity spectra of a Zone 2 deployment (Figure 2) divided into record lengths of 10 (a), 20 (b), 30 (c), and 60 (d) *min* with corresponding 95% chi-square confidence limits. Significant spectral peaks are highlighted (circles).

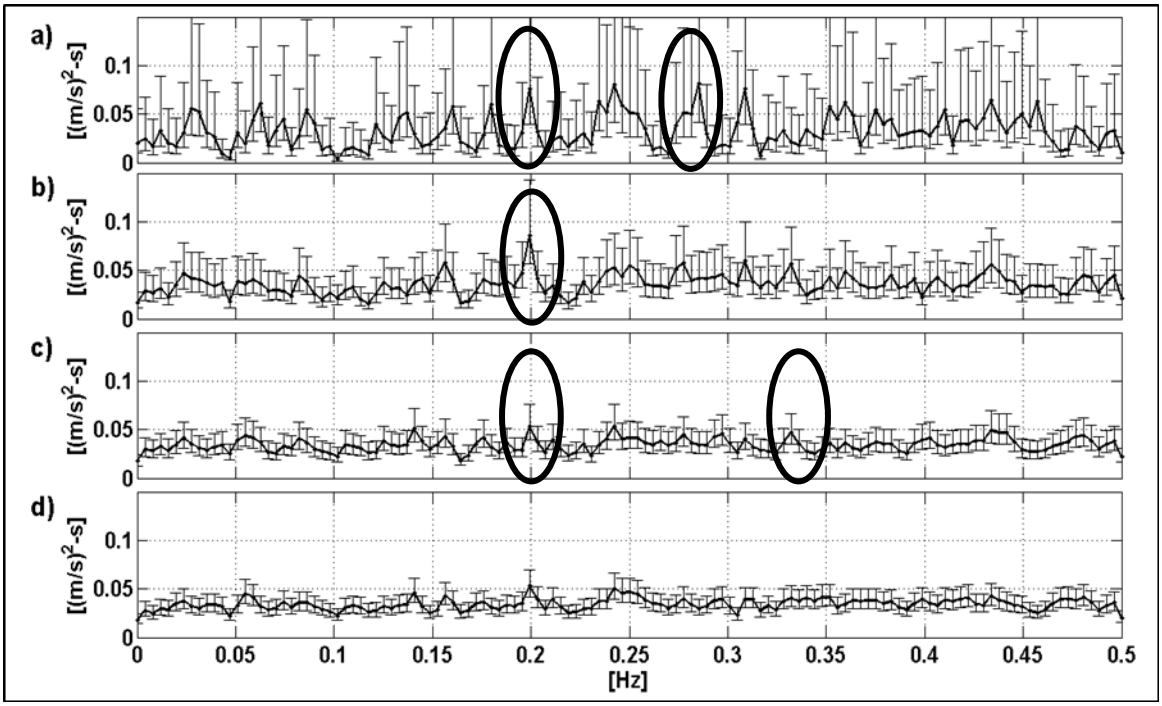

Figure 16. Spectra of a synthetic random Gaussian noise signal computed with different record lengths of 10 (a), 30 (b), 60 (c), and 90 (d) *min* with corresponding 95% chi-square confidence limits. Significant spectral peaks are highlighted (circles).

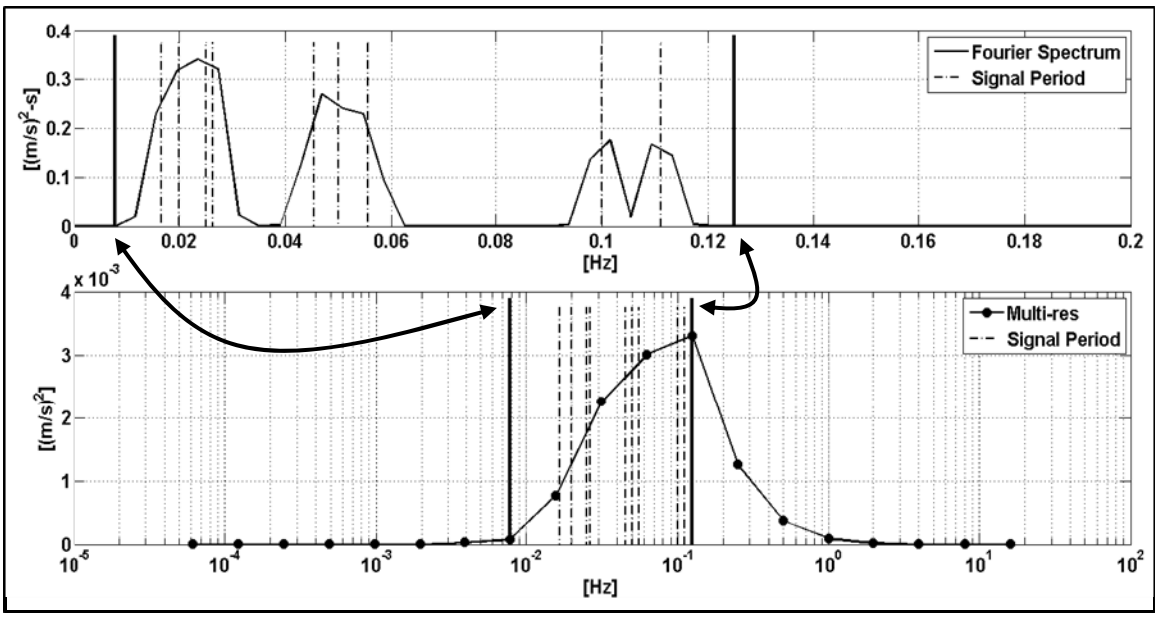

Figure 17. Fourier spectrum (top) and MR (bottom) of a synthetic signal composed of periodic signals. Vertical dashed lines represent corresponding frequencies of the signals. Solid vertical lines indicate frequency limits determined from MR.

Zone # /Yearday (2011)	***U* [m/s]**	***h* [m]**	**River feature**
1 / 221	1.52	0.63	Main channel
1 / 221	1.38	0.74	Main channel
1 / 224	1.63	0.78	Main channel
2 / 225	1.28	0.61	Main channel – upstream
2 / 225	1.47	1.03	Main channel – upstream
2 / 226	1.41	0.72	Main channel – upstream
3 / 227	0.59	1.70	Small channel
3 / 228	0.46	0.61	Small channel
4 / 222	0.57	1.19	Downstream of man-made structure
4 / 224	0.29	0.89	Downstream of man-made structure

Table 1. List of frame deployments and corresponding zones (Figure 2) used for data analysis with associated mean stream-wise velocity, *U*, depth of flow, *h*, and major river feature.

Zone #	***h* [m]**	***Lc* [m]**	***Tc* [s]**	***L/h***
1	0.63	5	3	8
	0.74	10	7	14
	0.78	8	5	10
2	0.61	8	6	13
	1.03	7	5	7
	0.72	10	7	14
3	1.70	20	33	12
	0.60	22	48	37
4	1.20	7	12	6
	0.89	22	73	25

Table 2. Linearly extrapolated coherent lengths, times, and length scales as a function of flow depth, *h*, for each zone (Figure 2).

Zone #	**ADCP Beam Length [m]**	***a) L* [m] (cs, turb)**	***b) L* [m] (cs, turb)**
1	*2.8	—, —	—, —
	4.2	—, —	—, 3.9
	4.9	—, —	—, 2.4
2	5.25	—, 3.2	—, 4.7
	3.85	—, —	—, 4.3
	6.3	—, —	—, 6.5
3	*10	—, 4.7	7.8, 4.7
	*9.5	—, 4.5	6.5, 3.9
4	*2	—, —	—, —
	3.5	—, 2.1	—, 2.4

Table 3. Motion lengths computed from f-k_s spectra using two times the ADCP beam length (a) and four times the ADCP beam length (b) for coherent flow structures (cs) and turbulence (turb) of each zone (Figure 2). Asterisks denote the beam length prevented the calculation of the full range of wavenumbers and lines indicate the wavenumbers are beyond resolvable limits.

Zone #	***h* [m]**	***T* [s]**	***L=UT* [m]**	***L/h***
1	0.63	30	45	71
	0.74	65	91	123
	0.78	36	58	74
2	0.61	35	45	74
	1.03	54	80	78
	0.72	40	56	78
3	1.70	74	44	26
	0.60	82	38	63
4	1.20	84	48	40
	0.89	87	25	28

Table 4. Length and temporal scales of the coherent flow structures in each zone (Figure 2) computed from Eqs. 1 and 2 using frequency limits determined from MR and energy spectra.

LIST OF REFERENCES

Adrian, R. J., 2007: Hairpin vortex organization in wall turbulence. *Phys. Fluids,* **19**, 041301, doi:10.1063/1.2717527.

Biltoft, C. A., and E. R. Pardyjak, 2009: Spectral Coherence and the Statistical Significance of Turbulent Flux Computations. *J. Atmos. Oceanic Technol.,* **25**, 403–410.

Bendant, J. S., and A. G. Piersol, 2000: *Random Data, Analysis and Measurement Procedures.* Wiley Interscience, 594 pp.

Buffin-Belanger, T., and A. G. Roy, 1998: Effects of a pebble cluster on the turbulent structure of a depth-limited flow in a gravel-bed river. *Geomorphology,* **25**, 249–267.

Buffin-Belanger, T., and A. G. Roy, 2005: 1 min in the life of a river: selecting the optimal record length for the measurement of turbulence in fluvial boundary layers. *Geomorphology*, **68**, 77–94.

Buffin-Belanger, T., A. G. Roy, and A. D. Kirkbride, 2000: On large-scale flow structures in a gravel-bed river. *Geomorphology*, **32**, 417–435.

Cantwell, B. J., 1981: Organized Motion in Turbulent Flow. *Ann. Rev. Fluid Mech,.* **13**, 457–515.

Capon, J., 1969: High-Resolution Frequency-Wavenumber Spectrum Analysis. *Proc. IEEE,* **57**, 1408–1418.

Carrasco, A., and C. A. Vionnet, 2004: Separation of scales on a broad, shallow turbulent flow. *J. Hydraul. Res.*, **42.6**, 630–638.

Dinehart, R. L., 1999: Correlative velocity fluctuations over a gravel river bed. *Water Resour. Res.,* **35**, 569–582.

Emery, W. J., and R. E. Thomson, 2001: *Data Analysis Methods in Physical Oceanography.* 2. Elsevier, 638 pp.

Fosness, R. L., and M. L. Williams, 2009: Sediment Characteristics and Transport in the Kootenai River White Sturgeon Critical Habitat near Bonners Ferry, Idaho. USGS Scientific Investigations Report 2009-5228, 40 pp.

Gunawan, B., M. Sterling, and D. W. Knight, 2010: Using an acoustic Doppler current profiler in a small river. *Water and Environment Journal*, **24**, 147–158.

Hardy, R. J., J. L. Best, S. N. Lane, and P. E. Carbonneau, 2009: Coherent flow structures in a depth-limited flow over a gravel surface: The role of near-bed turbulence and influence of Reynolds number. *J. Geophys. Res.,* **114**, F01003, doi:10.1029/2007JF000970.

Hardy, R. J., J. L. Best, S. N. Lane, and P. E. Carbonneau, 2010: Coherent flow structures in a depth-limited flow over a gravel surface: The influence of surface roughness. *J. Geophys. Res.,* **115**, F03006, doi:10.1029/2009JF001416.

Howell, J. F., and L. Mahrt, 1997: Multiresolution Flux Decomposition. *Boundary-Layer Meteorol.,* **83**, 117–137.

Lesht, B. M., 1980: Benthic Boundary-Layer Velocity Profiles: Dependence on Averaging Period. *J. Phys. Oceanogr.,* **10**, 985–991.

MacVicar, B. J., E. Beaulieu, V. Champagne, and A. G. Roy, 2007: Measuring water velocity in highly turbulent flows: field tests of an electromagnetic current meter (ECM) and an acoustic Doppler velocimeter (ADV). *Earth Surface Processes and Landforms,* **32**, 1412–1432.

Marquis, G. A., and A. G. Roy, 2006: Effect of flow depth and velocity on the scales of macroturbulent structures in gravel-bed rivers. *Geophys. Ret. Lett.,* **33**, L24406, doi:10.1029/2006GL028420.

Muste, M., K. Yu, T. Pratt, and D. Abraham, 2004: Practical aspects of ADCP data use for quantification of mean river flow characteristics; Part II: fixed-vessel measurements. *Flow Measurement and Instrumentation,* **15**, 17–28.

Nakagawa, H., and I. Nezu, 1981: Structure of space-time correlations of bursting phenomena in an open-channel flow. *J. Fluid Mech.,* **104**, 1–43.

Oltman-Shay, J., and R. T. Guza, 1984: A Data-Adaptive Ocean Wave Directional-Spectrum Estimator for Pitch and Roll Type Measurements. *J. Phys. Oceanogr.,* **14**, 1800–1810.

Oltman-Shay, J., and R. T. Guza, 1987: Infragravity Edge Wave Observations on Two California Beaches. *J. Phys. Oceanogr.,* **17**, 644–663.

Oltman-Shay, J., P. A. Howd, and W. A. Birkemeier, 1989: Shear Instabilities of the Mean Longshore Current 2. Field Observations. *J. Geophys. Res.,* **94**, 18031–18042.

Pawka, S. S., 1983: Island Shadows in Wave Directional Spectra. *J. Geophys. Res.,* **88**, 2579–2591.

Reniers, A. J. H. M., J. H. MacMahan, E. B. Thornton, and T. P. Stanton, 2006: Modelling infragravity motions on a rip-channel beach. *Coastal Engineering*, **53**, 209–222.

Robert, A., A. G. Roy, and B. DeSerres, 1996: Turbulence at a roughness transition in a depth limited flow over a gravel bed. *Geomorphology*, **16**, 175–187.

Roy, A. G., T. Buffin-Belanger, H. Lamarre, and A. D. Kirkbride, 2004: Size, shape and dynamics of large-scale turbulent flow structures in a gravel-bed river. *J. Fluid Mech.*, **500**, 1–27.

Shvidchenko, A. B., and G. Pender, 2001: Macroturbulent structure of open-channel flow over gravel beds. *Water Resour. Res.*, **37**, 709–719.

Sheremet, A., R. T. Guza, and T. H. C. Herbers, 2005: A new estimator for directional properties of nearshore waves. *J. Geophys. Res.*, **110**, C01001, doi:10.1029/2003JC002236.

Soulsby, R. L., 1980: Selecting Record Length and Digitization Rate for Near-Bed Turbulence Measurements. *J. Phys. Oceanogr.*, **10**, 208–219.

Sukhodolov, A. N., and W. S. J. Uijttewaal, 2010: Assessment of a River Reach for Environmental Fluid Dynamics Studies. *J. Hydr. Eng.*, **136**, 880–888.

Tamburrino, A., and J. S. Gulliver, 1999: Large flow structures in a turbulent open channel flow. *J. Hydraulic Research*, **37**, 363–380.

U.S. Geological Survey, cited 2010: National Water Information System: Web Interface. *USGS Real-Time Water Data for the Nation* 2010. [Available online at http://waterdata.usgs.gov/usa/nwis/nwisman/.]

Vickers, D., and L. Mahrt, 2003: The Cospectral Gap and Turbulent Flux Calculations. *J. Atmos. Oceanic Technol.*, **20**, 660–672.

Zaman, K. B. M. Q., and A. K. M. F. Hussain, 1981: Taylor hypothesis and large-scale coherent structures. *J. Fluid Mech.*, **112**, 379–396.

THIS PAGE INTENTIONALLY LEFT BLANK

INITIAL DISTRIBUTION LIST

1. Defense Technical Information Center
   Ft. Belvoir, Virginia

2. Dudley Knox Library
   Naval Postgraduate School
   Monterey, California

3. Professor Jamie MacMahan
   Naval Postgraduate School
   Monterey, California

4. Professor Ed Thornton
   Naval Postgraduate School
   Monterey, California

5. Professor Jeffrey Paduan
   Naval Postgraduate School
   Monterey, California